Cu nanoparticles enable plasmonic-improved silicon photovoltaic devices

PHYSICAL CHEMISTRY CHEMICAL PHYSICS, CAMBRIDGE, v. 14, n. 45, pp. 15722-15728, APR, 2012

PCCP

Cite this: *Phys. Chem. Chem. Phys.*, 2012, **14**, 15722–15728

www.rsc.org/pccp

PAPER

Cu nanoparticles enable plasmonic-improved silicon photovoltaic devices†

Michele L. de Souza,[ab] Paola Corio[a] and Alexandre G. Brolo*[b]

Received 2nd October 2012, Accepted 5th October 2012
DOI: 10.1039/c2cp43475j

This work examines the effect of copper nanoparticles (Cu NPs) on the photocurrent efficiency of silicon photovoltaic (Si PV) devices. An optimized synthesis of stable Cu NPs is reported together with a procedure for their immobilization on the Si PV surface. A comprehensive analysis of the photocurrent and power dependence of the Cu NPs surface coverage and size is presented. A decrease in photoconversion was observed for wavelengths shorter than ~500 nm, due to the Cu interband absorption. In the low surface coverage limit, where the level of aggregation was found to be low, the surface plasmon resonance absorption dominates leading to a modest effect on the photocurrent response. As the number of aggregates increased with the surface coverage, the photocurrent efficiency also increased, and a maximum enhancement power conversion of 16% was found for a 54 ± 6 NPs per μm^2 PV cell. This enhancement was attributed to SPR light scattering and trapping into the Si PV device. Higher surface coverage yielded numerous aggregates which acted as a bulk coating and caused a decrease in both photocurrent and power measurements.

Introduction

Photovoltaic (PV) devices are bound to play a major role in addressing our future energy needs.[1] However, the current generation of PVs still suffers from shortcomings that affect their viability as an economic alternative energy solution.[2] The main commercially relevant types of PVs are silicon (Si)-based, and they are classified as first and second generation cells.[2] The first generation cells are fabricated on approximately 300 μm thick monocrystalline or multicrystalline Si wafers. The second generation cells are constructed using 1 to 3 μm Si film deposited over a variety of materials, such as plastic, glass or metals. Second generation cells offer obvious advantages in terms of material costs.[2]

Light losses in Si PVs, due to surface reflectivity, poor absorption or scattering processes, are considered one of the issues that need to be overcome. Improved light absorption and trapping in first generation Si PVs are achieved by surface texturing.[3] This procedure is available for thick solar cells that can afford ~5–10 μm of Si removal in order to yield a structured surface.[3] Texturing promotes light trapping through internal scatterings which enhances the light endurance in the device. This strategy is not as convenient for second generation, thin film, Si PVs. In that case, texturing by generating surface irregularities results in increased electron–hole (e^-–h^+) pair recombination, which is a loss mechanism that correlates with the increased surface area.[4] Anti-reflection (AR) coating is also implemented in PVs to improve light absorption.[5]

Alternative strategies concerning the light trapping and absorption on both first and second generation Si PVs are an active area in solar cell research. Plasmonic integration with solar cells corresponds to one of the most promising approaches to address the light absorption and trapping issues.[6] Plasmonic structures are metallic nanomaterials that support surface plasmon resonances (SPR), which are collective oscillations of the conducting electrons in those subwavelength structures. Incident light that matches the SPR energy is strongly scattered and absorbed, and the magnitude of the extinction (the term "extinction" means the combination of these two processes: scattering + absorption) depends on the geometric characteristics of the structure, such as size and shape of the metallic nanoparticles (NPs).[7] These are features that can be tuned by the appropriate fabrication procedure. The plasmonic properties are well-known to improve spectroscopic properties for species adsorbed on metallic surfaces, such as in the surface-enhanced Raman scattering (SERS) effect.[7,8]

The application of plasmonics to improve photocurrent response in PV devices is currently a very active research area.[9–11] Stuart and Hall pioneered this field by employing ~100 Å thick Au, Ag and Cu (metals that support SPR in the visible range) annealed islands, over a thin silicon-on-insulator (SOI) device.[9,12] The presence of the metallic nanoparticles

[a] *Instituto de Química, Universidade de São Paulo, Av. Prof. Lineu Prestes, 748, Cidade Universitária, 05513-970, São Paulo, SP, Brazil. E-mail: michele.souza@usp.br, paola@iq.usp.br; Fax: +55 11 3091 3890; Tel: +55 11 3091 3853*
[b] *Department of Chemistry, University of Victoria, V8W 3V6, P.O. Box 3065, Victoria, BC, Canada. E-mail: agbrolo@uvic.ca; Fax: +1 250 721-7147; Tel: +1 250 721-7167*
† Electronic supplementary information (ESI) available. See DOI: 10.1039/c2cp43475j

was correlated to an increase of the photocurrent response, which was associated with the SPR of the nanostructures. Polman and Catchpole demonstrated that, under SPR conditions, a silver nanoparticle (Ag NP) placed at a Si–air interface will scatter light preferentially into the higher refractive index material.[13] The fraction of the scattered light into the material depends on the nanoparticle shape (spheres, hemisphere, cylinder and dipole were studied).[4] The importance of the distance between the metallic nanoparticle and the Si substrate was also discussed.[4,6] Schaadt *et al.* reported a slight improvement on the photocurrent response of a Si wafer-based device at approximately 900 nm due to the presence of gold nanoparticles (Au NPs), deposited as a drop of colloidal suspension at the surface. A 2-fold improvement in the photocurrent was further observed at wavelengths that matched the SPR for 50 and 80 nm diameter Au NPs.[14,15] Catchpole *et al.* reported a 7-fold enhancement at 1200 nm on photocurrent response of a wafer-based solar cell (first generation PV) containing annealed Ag NPs (10 to 18 nm diameters) and 16-fold enhancement for a thin-film SOI device.[16] Although the photocurrent response curves showed enhancements in the low energy region, in some cases an increase was also observed at the SPR region for both Au NPs and Ag NPs in the visible range.

All these results are promising indicators of the potential of plasmonics as a tool for improving solar cell efficiency. However, the availability and cost of Au and Ag, the most explored metallic materials so far in plasmonic PV research, are generally identified as possible drawbacks to the widespread implementation of the plasmonic approach. On the other hand, Cu is a plasmonic material that is more abundant and less expensive than Ag and Au, and might constitute a potential alternative for the commercialization of the plasmonic technology. Cu nanostructures have lagged behind Au and Ag in terms of plasmonic applications due to its low chemical stability and less efficient SPR. Although nanostructured Cu islands deposited on Si devices showed the best enhanced photocurrent response (maximized at 800 nm), compared to Au and Ag islands.[9]

The goal of this work is to report a comprehensive investigation on the effect of Cu NPs on the efficiency of solar cell devices. Wafer-based, first generation, silicon solar cells were used because they are widely available and have good photocurrent response. In that case, however, their p–n junction is buried deep in the device and they do not benefit from any field localization effects.[16] The results are then interpreted in terms of scattering efficiency and light trapping into the devices. The approach consisted of wet chemistry deposition of Cu NPs through a self-assembly layer of 3-aminopropyltrimethoxysilane (APTMS). This is a relatively simple and low cost procedure that might be promising to future plasmonic PV applications.

Experimental section

Equipment and materials

Copper(II) nitrate trihydrate ($Cu(NO_3)_2{\cdot}3H_2O$, 98% purity), sodium citrate dihydrate ($C_6H_5O_7Na{\cdot}2H_2O$, purity > 99%), sodium borohydride ($NaBH_4$, purity > 96%), sodium hydroxide (NaOH, purity > 98%) and 3-aminopropyltrimethoxysilane (APTMS, 97% purity) were purchased from Sigma-Aldrich and used without further purification.

Si PV samples (2×2 cm^2) constituted of approximately 200 ± 20 μm thick multicrystaline Si, boron-positively doped, with rear aluminium contacts and Al front fingers contacts (resistances measured with 2 probes 1 cm apart were between 25 and 57 Ω). They were provided by Yangzhou Huaer Solar-PV Technology Co., Ltd.

A Newport lamp (Xe, Hg, Hg(Xe) arc, 50–500 W, model 67005) and an AM 1.5 filter were employed as a light source in order to emulate solar radiation. The samples photocurrent and power efficiency were measured employing a Cary Techtron Sirospec monochromator (0.5 μm grating, range between 380 and 850 nm, and 10 nm resolution), a 510 nm Kodak cutoff filter was employed for irradiation above 600 nm, a PerkinElmer chopper model 650 at 500 Hz connected to an EG&G Signal Recovery lock-in amplifier model 7265 DSP and a Princeton Applied Research (PAR) potentiostat/galvanostat model 173. The data were acquired using a customized program written using Labview 8.1 software. External Quantum Efficiency measurements (EQE) were obtained from a QEX7 Solar Cell Spectral Response (PV Measurements Inc.) at Day4 Energy Inc (www.day4energy.com). A 8G017 photodiode and integrating sphere coupled to QEX7 were employed in reflectance spectra acquisition (setup customized for Day4 Energy). Scanning electron microscopy (SEM) images were acquired on a Hitachi S-4800 scanning microscope, an accelerating voltage and a current of 1 kV and 10 μA respectively. UV-VIS measurements were acquired using a Varian Cary 50 Scan UV-visible spectrophotometer.

Cu NPs synthesis

Cu NPs were synthesized in aqueous solution based on a method previously reported by Sánchez-Cortéz[17] with modifications that improved the yield of the synthesis and the stability of the Cu NPs. The reaction atmosphere was controlled using high pressure nitrogen flow. The Cu NPs synthesis consisted of adding freshly prepared 1667 μL of 1.0×10^{-2} mol L^{-1} copper(II) nitrate to 20 mL of 5.6×10^{-3} mol L^{-1} sodium citrate dihydrate aqueous solution in an Erlenmeyer at room temperature under intense stirring. This solution was purged with nitrogen for 30 minutes, in order to remove dissolved gases and saturate the solution with nitrogen, followed by the addition of 10 mL of an aqueous solution containing 2.0×10^{-2} mol L^{-1} sodium hydroxide and 2.0×10^{-2} mol L^{-1} sodium borohydride. The Cu NPs synthesis was performed under a nitrogen atmosphere and monitored by UV-VIS spectroscopy.

Cu NPs immobilization on Si PV samples

The Cu NPs immobilization (Scheme 1) was preceded by the adsorption of APTMS on the surface of the Si PVs. Cleaned and dried Si PV samples were placed vertically into 1% APTMS ethanolic solution for 30 minutes at room temperature. The procedure allowed efficient chemisorption of APTMS and did not lead to significant changes in the electric properties of the PVs.[18] After the APTMS adsorption procedure, the samples

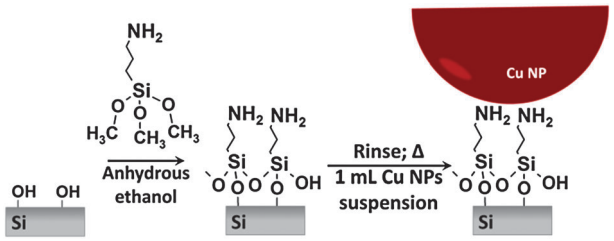

Scheme 1 Representation of the APTMS self-assembly layer formation and Cu NPs immobilization on Si PVs.

were abundantly rinsed with anhydrous ethanol and water, dried under nitrogen flux and kept in an oven at 100 °C for 20 minutes to remove traces of solvent.

1 mL of the Cu NPs suspension was deposited on the surface of the APTMS modified Si PVs. The PV samples were kept in contact with the Cu NPs suspension for a pre-determined time (10, 15, 30, 45, 60 and 90 minutes), rinsed with deionized water and dried with a stream of nitrogen. The size of the Cu NPs and surface coverage on the PV devices were analysed by SEM right after the photocurrent and power measurements.

Results and discussion

Cu NPs synthesis and stability

The Cu NPs synthesis under a nitrogen environment yielded a stable brown suspension characterized by a SPR peak at approximately 569 nm (Fig. 1(A)). Cu NPs fabricated in an oxidative environment (in the absence of the nitrogen flux) yielded a dark-green suspension, presenting a red shift in the SPR band to 590 nm and an additional broad extinction at 750 nm (dashed line, Fig. 1(A)). The 750 nm band is characteristic of the exciton absorption of copper(I) oxide (Cu_2O).[19] The observed ~20 nm red-shift in the SPR band can be assigned to the presence of a Cu_2O layer that affects the dielectric properties surrounding the metallic Cu core ($Cu@Cu_2O$).[19–21] The NPs prepared in an oxidative environment were unstable, and were completely precipitated after a short period of time (~3 hours).

The time evolution of the synthesis of Cu NPs suspension was monitored by UV-VIS spectroscopy (Fig. 1(A) and (B)). The SPR peak intensity at 569 nm in the extinction spectra increased with the reaction time (Fig. 1(A)). A shoulder at 360 nm, indicated in Fig. 1(A), developed after 90 minutes of reaction and it is attributed to an interband transition in nanocrystalline Cu_2O.[20] The Cu_2O band-to-band transition (~360 nm) is evident only at the end of the process. The presence of this band was confirmed by a proper baseline treatment following spectral deconvolution, as presented in Fig. S1 (ESI†). The increasing extinction background from 500 nm towards the blue is attributed to the metallic Cu interband transition.[22]

Although CuO is the most stable form of bulk copper oxides, earlier studies indicated that nanoscale Cu_2O is also relatively stable and does not convert to CuO. A few nanometers of Cu_2O were shown to act as a barrier that slows the oxygen diffusion into Cu NPs.[20] The integrity of our Cu NPs was maintained in air for approximately 5 hours after the synthesis, suggesting that the particles were a core@shell

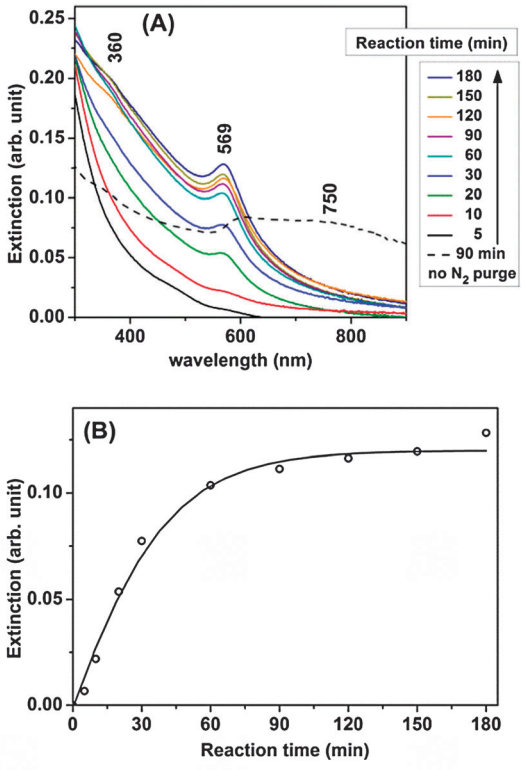

Fig. 1 (A) Extinction (absorption + scattering) spectra of Cu NPs under slightly positive nitrogen pressure as a function of the indicated reaction time (dashed line: 90 minute reaction performed without nitrogen flux); (B) extinction at 569 nm as a function of the reaction time for the reactions under a stream of nitrogen. (1 mm cuvette path length, aqueous solution, nitrogen saturated).

structure.[19,20] The NPs can be stable for days if the suspension is maintained under nitrogen.

The intensity of the 569 nm SPR band is plotted against the reaction time in Fig. 1(B). The intensity of the SPR band increased during the first 90 minutes of reaction (Fig. 1(B)) indicating an increase in the amount of Cu NPs in suspension within that time frame. Cu NPs immobilization onto the Si PVs was performed using suspensions prepared after 90 minutes of reaction (plateau in Fig. 1(B)). This ensured that the concentration of Cu NPs was similar in all experiments.

SEM images are shown in Fig. 2 for four different Si PV surfaces containing immobilized Cu NPs. The immobilized Cu NPs presented low polydispersity, but a degree of agglomeration in some cases. Nine Si PV samples with distinct surface coverage were analysed, revealing an average Cu NPs diameter around 21.2 ± 4.9 nm. The size distributions, also shown in Fig. 2, were used to correlate the surface coverage and the presence of Cu NPs aggregates to the photogenerated current and power in each of the solar cells.

Short-circuit current density and external quantum efficiency measurements

Reflectance spectra from a Si PV surface before and after the Cu NPs immobilization (surface coverage of 14 ± 4 NPs per μm^2) is presented in Fig. 3(A). The amount of reflected light decreased for all wavelengths after the Cu NPs immobilization. The larger

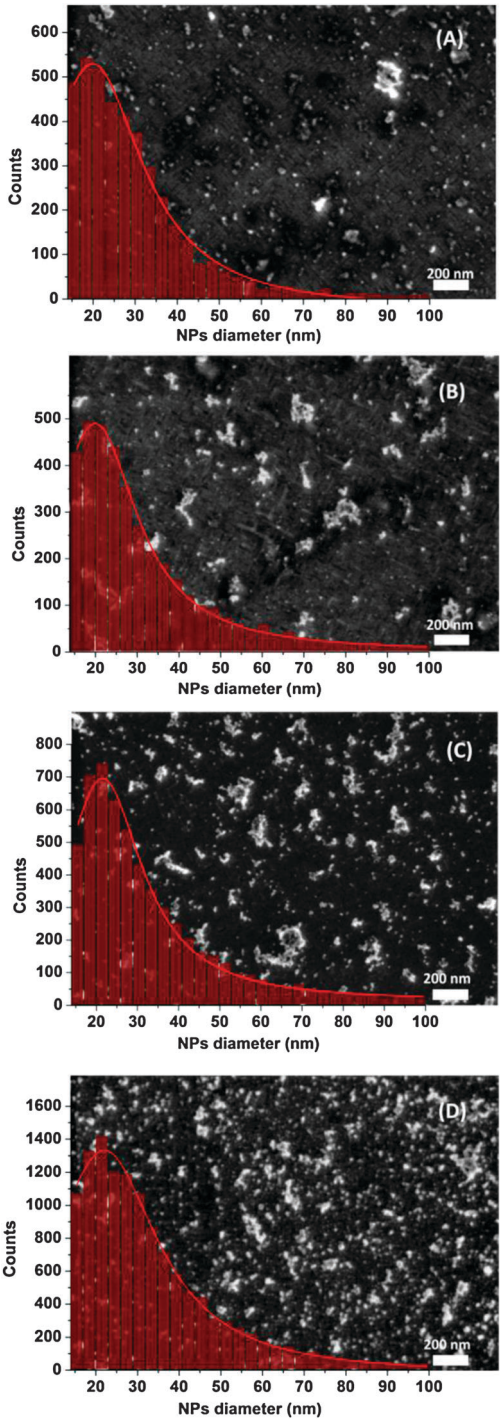

Fig. 2 SEM images of the Si solar cells after Cu NPs immobilization. Surface coverage: (A) 48 ± 17; (B) 52 ± 11; (C) 81 ± 17; and (D) 135 ± 32 NPs per μm^2. The distribution size histograms are shown as inset in each image.

decrease in reflectivity due to the Cu NPs modification occurred at wavelengths below 400 nm, and is corroborant with the UV-VIS spectra in Fig. 1(A). The increased extinction below 400 nm has been assigned to the interband transition of metallic Cu and to the band-to-band transition from the nanocrystalline Cu_2O. The effect of the Cu NPs on the Si PV reflectance for wavelengths longer than 400 nm is attributed to

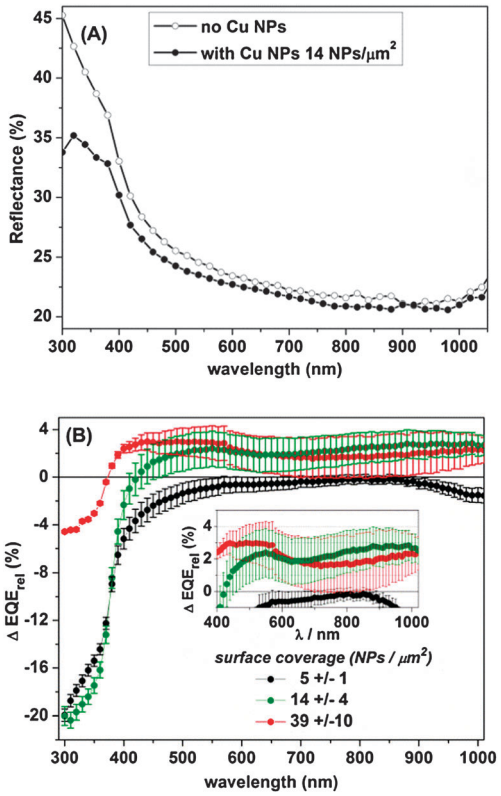

Fig. 3 (A) Reflectance spectra from a Si PV sample before and after Cu NPs immobilization. The Si PV surface was first modified with APTMS, as described in the text; (B) Relative External Quantum Efficiency variation (ΔEQE_{rel}, calculated according to eqn (1)) at different wavelengths for three distinct surface coverages, as indicated in the figure (the figure inset presents a zoomed view for a range of wavelengths). The error bars were calculated from measurements obtained at different regions of the Si PVs.

the preferential scattering and trapping into the solar cells. The plasmonic characteristics of the cell in the visible range were emphasized by calculating the difference spectrum showed in Fig. S2 (ESI†).

External quantum efficiency (EQE) measurements were acquired for Si PVs before and after both APTMS self-assembly and Cu NPs immobilization. The EQE curves after APTMS assembly overlapped with the results obtained from the bare Si PV, confirming that the presence of APTMS does not significantly alter the electric properties of the solar cells. EQE relative variations (ΔEQE_{rel}) were obtained for all wavelengths covered, according to eqn (1) below:

$$\Delta EQE_{rel} = \frac{EQE_{Cu} - EQE_{APTMS}}{EQE_{APTMS}} \times 100 \qquad (1)$$

EQE_{APTMS} and EQE_{Cu} are the EQE of the Si PVs before and after the Cu NPs immobilization, respectively. Increases in the photocurrent conversion efficiency between 2.0 and 3.5%, in the 400 to 1000 nm wavelength range, were observed after the Cu NPs immobilization for surface coverage of 14 ± 4 and 39 ± 10 NPs per μm^2 (Fig. 3(B) inset). The Si PV sample with surface coverage equals to 5 ± 1 NPs per μm^2 showed no EQE increase for all wavelengths (Fig. 3(B) inset). An intense damping of the EQE is observed in Fig. 3(B) for all Si PV

samples for wavelengths below 400 nm. This decrease can be associated with the interband transition of metallic Cu, which is evident in the reflectance spectrum of Fig. 3(A). The error bars are associated with the spatial variations in the response of the multicrystalline Si PVs. The EQE measurements were performed in different regions of the PVs and averaged. The average EQE signal shows a consistent increase for the solar cells modified with Cu NPs.

EQE and short-circuit current density (J_{sc}) are equivalent measurements in the context of this work and they yield the same information (see a justification for this statement in the ESI† file). Relative variations, defined in eqn (2), were also evaluated for the J_{sc} for another set of samples comprising a larger range of surface coverage (from 48 ± 17 NPs per μm^2 to 135 ± 32 NPs per μm^2).

$$\Delta J_{sc\ rel} = \frac{J_{sc\ Cu} - J_{sc\ APTMS}}{J_{sc\ APTMS}} \times 100 \qquad (2)$$

where $J_{sc\ APTMS}$ and $J_{sc\ Cu}$ are the J_{sc} before and after the Cu NPs immobilization, respectively. The results for the relative J_{sc} variations are presented in Fig. 4.

The map in Fig. 4 presents a maximum increase of 2% for the J_{sc} in the visible range for Si PV samples with a surface coverage from 48 to 52 Cu NPs per μm^2. An increase in the short-circuit photocurrent density of about 8 to 12% relative to the photocurrent density obtained in the absence of the NPs was recorded in the near infrared (750 nm) for the lower surface coverage investigated. As the surface coverage increased beyond 52 Cu NPs per μm^2, small and sporadic variations in the $\Delta J_{sc\ rel}$ were measured in the visible. The 94 NPs per μm^2 sample was an exception in this trend and presented increases of 4% in the 450 to 750 nm region. The 84 and 99 NPs per μm^2 samples showed about 4% J_{sc} increase relative to the samples without NPs in the near IR at approximately 800 nm.

The observed J_{sc} increases in Fig. 4 did not match the specific wavelengths related to the SPR band of the Cu NPs in aqueous solution (569 nm). The maximum increase in the J_{sc} occurred in the near IR, in agreement to previous reports.[9,14,16] The reflectance spectrum, Fig. 3(A), did not show observable evidence of preferential SPR excitation at 569 nm; however, an extinction peak at 850 nm is observed in the subtracted reflection spectra shown in Fig. S2 (ESI†).

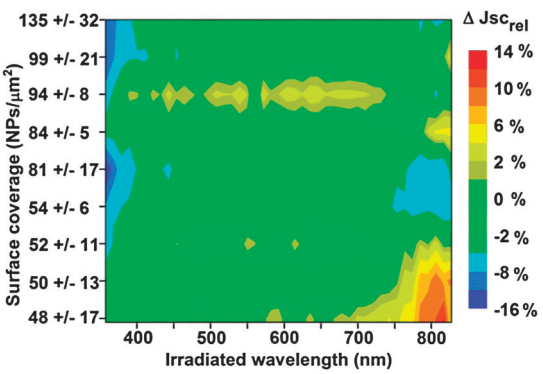

Fig. 4 Relative J_{sc} variation ($\Delta J_{sc\ rel}$ - defined in eqn (2)) map as a function of the surface coverage and irradiated wavelength.

The oxide layer in the vicinity of the Cu NPs is expected to red-shift the SPR due the dielectric changes on the metal surroundings relative to the aqueous environment. Notice that the Cu NPs were exposed to air during the Si PV measurements, which should lead to a thicker oxide layer than for the NPs in the nitrogen-purged aqueous solution. This assumption is corroborated by Pal *et al*. who investigated the dependence of the size and oxide shell thickness on the Cu NPs SPR. It was demonstrated that the SPR band suffers a decrease in intensity that depended on the thickness of the oxide layer, together with a red-shift in the SPR maxima.[21] The red-shift of the Cu NPs SPR to the near IR is an advantage, since it takes the resonance away from the region of interband transition. The presence of aggregates also red-shifts and broaden the SPR band.

The intense J_{sc} damping at wavelengths below 500 nm to samples with surface coverage between 52 and 135 NPs per μm^2 (Fig. 4) is again assigned to the Cu interband transition.

The effect of Cu NPs on the power efficiency of Si PVs

Power measurements (using white light from the Xe light source coupled to the AM 1.5 filter) were performed for all Si PV samples before and after Cu NPs immobilization (power measurements before and after the self-assembly of APTMS did not present any significant changes). Fig. 5(A) is an example of a power curve obtained for a surface coverage of 54 ± 6 NPs per μm^2. The *J*–*V* and power curves for all samples are available in Fig. S3 (ESI†). The power curves were dependent on the surface coverage. The relative variation of the maximum power, defined in eqn (3), extracted from each Si PV cell investigated is presented in Fig. 5(B).

$$\Delta \mathrm{Power}_{rel} = \frac{\mathrm{Power}_{Cu} - \mathrm{Power}_{APTMS}}{\mathrm{Power}_{APTMS}} \times 100 \qquad (3)$$

Power_{Cu} and Power_{APTMS} are the maximum powers generated by white light illumination, using a solar cell emulator, in the presence and absence of copper nanoparticles, respectively.

The Cu NPs modified Si PV cells presented a power increase from about 8.0% to 16.4% relatively to the power in the absence of Cu NPs for certain surfaces coverage, in agreement with the J_{sc} enhancements presented in Fig. 4. It is important to notice that the J_{sc} measurements were limited by the range of the monochomator, which restricted the measurements from 380 nm to 850 nm and, did not capture the effect of higher wavelength photons. The maximum J_{sc} improvement for the Si PVs coated with Cu NPs ranging from 48 to 54 NPs per μm^2 (Fig. 4) shifted to the near infrared as the surface coverage increased, and the enhancement in power (Fig. 5(B)) seems to follow the same trend. Hence, although the 54 NPs per μm^2 did not show apparent J_{sc} improvement within the analysed wavelength range, the increased power observed under white light may be related to enhanced excitations in the near IR.

A decrease in power is observed in Fig. 5(B) for surface coverages larger than 54 NPs per μm^2, in agreement to the J_{sc} data shown in Fig. 4. Although the Cu NPs presented a relatively narrow size distribution, large NPs aggregates were more evident for high surface coverages (Fig. 2(A)–(D)). As the amount of Cu NPs at the surface increases, and a large

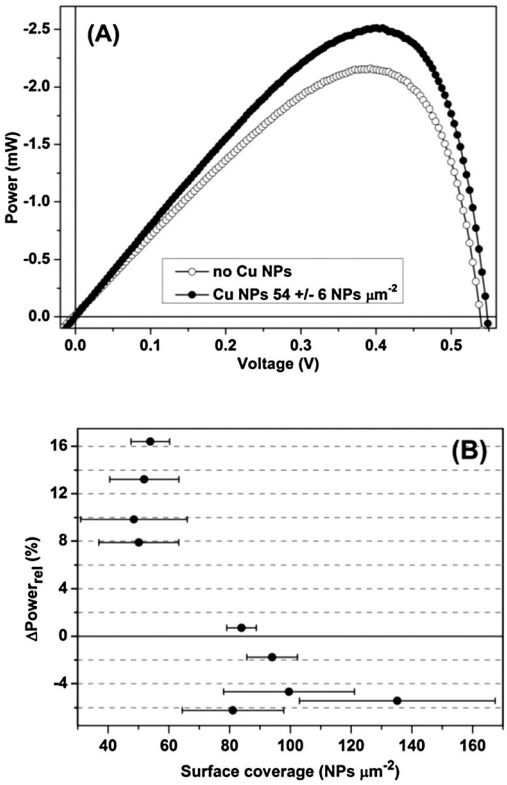

Fig. 5 (A) Si PV power curves (white light irradiated) before and after Cu NPs immobilization; (B) relative power variation ($\Delta Power_{rel}$ – defined in eqn (3)) for Si PV cells coated with Cu NPs at different surface coverages.

number of aggregates are observed; the characteristics of the coating shift towards bulk Cu. The metallization blocks the surface and impedes the light from entering the solar cells. The power decrease under high surface coverage can then be assigned to the bulk characteristics of large sized Cu NPs aggregates.

The effect of the copper oxidation on the stability of the cell was investigated by recording the power generation of a Cu NP coated PV device seven days after the NP deposition. The results, presented in Fig. S4 (ESI†), showed less than 1.5% in performance deterioration. This modest decrease in power generation can be attributed to the presence of the copper oxide layer that protected the core of the NPs against further oxidation. In any case, it is suggested that a protective transparent layer should be required in any attempt of practical implementation of copper as a plasmonic material for Si PV devices, as described in this work.

Summary of the effect of Cu NPs on the efficiency of Si PVs

The extinction from plasmonic structures (absorption and scattering of light) is both wavelength and size-dependent. The SPR extinction is dominated by absorption in small particles, while scattering effects are favoured in large aggregates. Fig. 3(B) and 4 highlight the dependence of the plasmonic effect on the PV efficiency with the irradiated wavelength.

Cu interband transition occurs at wavelengths shorter than 500 nm. This strong absorption restricts the amount of radiation that reaches the PVs' interior (Fig. 6(A)) and leads to

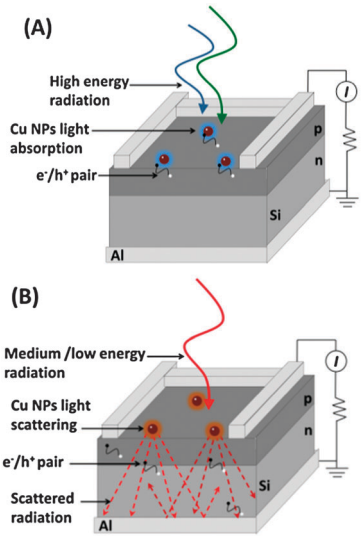

Fig. 6 Si PV representations: (A) the presence of Cu NPs enables the increase of light absorption at the surface; and (B) Cu NPs induce light scattering into the device at specific irradiated wavelengths.

decreased efficiency at shorter wavelengths for all PV devices coated with Cu NPs. A similar effect has been reported in the literature for small metallic NPs at the SPR. At low surface coverages, with the occurrence of only few aggregates, most of the Cu NPs were dispersed and there was low intensification of the ΔEQE_{ref} (Fig. 3(B)). In this case, absorption dominates the SPR, restricting the light to access the active layer of the device.

SPR red-shift, broaden and higher orders multipole excitation modes are observed in aggregated structures.[23] The red-shift of SPR due to aggregation and oxide layer growth on Cu NPs might be beneficial because it moves the plasmonic effect away from the Cu interband transition. At longer wavelengths, when scattering dominates the NPs' extinction (larger NP aggregates), PV light trapping is favoured through internal reflections (illustrated in Fig. 6(B)). The internal scattering increases the probability of e^{-}–h^{+} formation at the p–n junction. Surface coverages ranging from ~48 to 54 NPs per μm^2 presented a degree of agglomeration (Fig. 2(A) and (B)) which were correlated to enhancements in photocurrent and power (Fig. 4 and 5(B)). This enhanced efficiency can be attributed to plasmonic scattering of light into the PV devices.[11]

However, at higher surface coverage (~81 and 135 NPs per μm^2), the high number of aggregates (Fig. 2(C) and (D)) acted as a surface blocking coating. This "bulk effect" (metallization) decreased the PV photocurrent and power (Fig. 4 and 5(B)).

Conclusions

Cu NPs synthesized under nitrogen flux were stable and characterized by a SPR peak at 569 nm. The presence of a thin oxide layer was evident by an absorbance peak at 360 nm. The NPs are then better described as $Cu@Cu_2O$ and the position of the SPR band is dependent on the thickness of the copper oxide film.

The immobilization of Cu NPs on the surface of Si PV cells demonstrated to be an easy, simple and low cost procedure, and led to improvements in both short-circuit current density and power. The Si PV samples with a Cu NPs surface coverage ranging from 48 to 52 NPs per μm^2 triggered J_{sc} improvements of approximately 2% in the visible range and 8 to 12% improvements in the near IR relative to the photocurrent obtained in the absence of the NPs. A maximum of 16% increase in the power generated by the Si PV cells under white light illumination was also observed in the same surface coverage range. J_{sc} and EQE damping were observed for wavelengths below 400 nm and they were assigned to the metallic Cu interband transition. This effect was more important for high NPs surface coverage. A power decrease under white light illumination at high surface coverages was also observed, and assigned to the presence of large aggregates at the Si PV surface.

Although the use of Cu NPs in plasmonics PV has not been widespread due to the Cu poor chemical stability and losses due to the absorption at high energies (Cu interband transition), the improvement in power reported here indicated that Cu NPs might be promising plasmonic material that can play an important role in commercial PVs.

Acknowledgements

We thank Day4 Energy for technical support. M. L. S. acknowledges fellowships from the Department of Foreign Affairs and International Trade Canada (DFAIT) through the Emerging Leaders in the Americas (ELAP) program and from the CIAM-FAPESP program. P.C. also thanks the CNPq for a research fellowship. This work was supported by NSERC and by the University of Victoria. The authors also thank Milton Wang for his help in finding a supplier for the bare Si PV samples, and Luis Netter for his help with the development of the data acquisition software. The technical support from Dr Bram Sadlik with the measurements at Day4 Energy was greatly appreciated.

References

1 M. A. Green, *Prog. Photovolt.: Res. Appl.*, 2005, **13**, 447.
2 M. A. Green, *Sol. Energy*, 2004, **76**, 3.
3 D. H. Macdonald, A. Cuevas, M. J. Kerr, C. Samundsett, D. Ruby, S. Winderbaum and A. Leo, *Sol. Energy*, 2004, **76**, 277.
4 K. R. Catchpole and A. Polman, *Appl. Phys. Lett.*, 2008, **93**, 191113.
5 R. W. Miles, K. M. Hynes and I. Forbes, *Prog. Cryst. Growth Charact. Mater.*, 2005, **5**, 1.
6 H. A. Atwater and A. Polman, *Nat. Mater.*, 2010, **9**, 205.
7 K. L. Kelly, E. Coronado, L. L. Zhao and G. C. Schatz, *J. Phys. Chem. B*, 2003, **107**, 668.
8 M. Moskovits, *Rev. Mod. Phys.*, 1985, **57**(3), 783; M. Fan, G. F. S. Andrade and A. G. Brolo, *Anal. Chim. Acta*, 2011, **693**, 7.
9 H. R. Stuart and D. G. Hall, *Appl. Phys. Lett.*, 1996, **69**(16), 2327.
10 K. L. Chopra, P. D. Paulson and V. Dutta, *Prog. Photovoltaics Res. Appl.*, 2004, **12**, 69; Y. Tian and T. Tatsuma, *J. Am. Chem. Soc.*, 2005, **127**, 7632.
11 S. C. Warren and E. Thimsen, *Energy Environ. Sci.*, 2012, **5**, 5133.
12 H. R. Stuart and D. G. Hall, *Appl. Phys. Lett.*, 1998, **73**, 3815.
13 K. R. Catchpole and A. Polman, *Opt. Express*, 2008, **16**, 21793.
14 D. M. Schaadt, B. Feng and E. T. Yu, *Appl. Phys. Lett.*, 2005, **86**, 063106.
15 E. T. Yu, D. Derkacs, S. H. Lim, P. Matheu and D. M. Schaadt, *Plasmonics: Nanoimaging, Nanofabrication, and Their Applications IV (Proceedings Volume)*, 2008, vol. 7033.
16 S. Pilai, K. R. Catchpole, T. Trupke and M. A. Green, *J. Appl. Phys.*, 2007, **101**, 093105.
17 S. Sánches-Cortéz, J. V. García-Ramos and G. Morcillo, *J. Colloid Interface Sci.*, 1994, **167**, 428.
18 A. K. Chauhan, D. K. Aswal, S. P. Koiry, S. K. Gupta, J. V. Yakhmi, C. Sürgers, D. Guerin, S. Lenfant and D. Vuillaume, *Appl. Phys. A: Mater. Sci. Process.*, 2008, **90**, 581.
19 K. P. Rice, E. J. Walker Jr., M. P. Stoykovich and A. E. Saunders, *J. Phys. Chem. C*, 2011, **115**, 1793.
20 M. Yin, C.-K. Wu, Y. Lou, C. Burda, J. T. Koberstein, Y. Zhu and S. O'Brien, *J. Am. Chem. Soc.*, 2005, **127**, 9506.
21 O. Peña-Rodriguez and U. Pal, *J. Opt. Soc. Am. B*, 2011, **28**, 2735.
22 H. Ehrenreich and H. R. Philipp, *Phys. Rev.*, 1962, **128**, 1622.
23 V. Giannini, A. I. Fernández-Domínguez, S. C. Heck and S. A. Maier, *Chem. Rev.*, 2011, **111**, 3888.

